In: Wagner W., Székely, B. (eds.): ISPRS TC VII Symposium – 100 Years ISPRS, Vienna, Austria, July 5–7, 2010, IAPRS, Vol. XXXVIII, Part 7B

Contents   Author Index   Keyword Index

AIRBORNE HYPERSPECTRAL IMAGE GEOREFERENCING AIDED BY HIGH-RESOLUTION SATELLITE IMAGES

C. K. Toth [a,b] *, J.H. Oh [b], D. A. Grejner-Brzezinska [b]

[a] Center for Mapping, The Ohio State University, Columbus, Ohio, USA toth@cfm.ohio-state.edu
[b] Satellite Positioning and Inertial Navigation (SPIN) Laboratory, Dept. of Civil and Environmental Engineering and Geodetic Science, The Ohio State University, Columbus, Ohio – (oh.174, dbrzezinska)@osu.edu

Commission VII, WG VII/4

KEY WORDS: Georeferencing, Hyperspectral imagery, High-resolution satellite images, Image matching, Pushbroom camera

ABSTRACT:

Over the past decade, airborne hyperspectral systems have shown remarkable performance in identifying and classifying a variety of ground objects, such as differentiating between minerals, vegetations, artificial materials, water, etc. Though the hyperspectral imaging market is still relatively small, yet it is steadily growing. Currently, most of the high performance systems are of the pushbroom camera type, and consequently, the sensor orientation of these systems heavily relies on the integrated GPS/INS (Global Positioning System/Inertial Navigation System) based direct georeferencing solution. In this study, an indirect georeferencing method is proposed that is based on utilizing robust image matching to high-resolution satellite imagery. This solution can be used in circumstances where GPS/INS-based georeferencing is not available or not feasible due to GPS signal loss and/or the lack of GPS infrastructure. The proposed method is motivated by the attractive properties of state-of-the-art high-resolution satellite imagery, including large swath width, high spatial and temporal resolution, and high positional accuracy. For robust image matching, a combination of SURF (Speeded-Up Robust Features) and RANSAC (RANdom SAmple Consensus) is utilized, and the trajectory modeling of the airborne hyperspectral pushbroom camera is based on the collinearity equation camera model with the Gauss-Markov stochastic error model. Tests on simulation data showed encouraging performance results for the proposed approach.

1. INTRODUCTION

Over the past decade, airborne hyperspectral imaging (HSI) systems have shown excellent performance in several applications to identify and classify a broad range of ground objects, including minerals, vegetations, artificial materials, and water etc. Airborne HSI sensors measure the light from the earth's surface in high spectral resolution; typically, each pixel of hyperspectral data contains dozens or hundreds of spectral bands. HSI technology has been used in many commercial and defence applications.

Airborne HSI systems are predominantly based on the pushbroom camera model, which heavily relies on direct georeferencing. Typically, the georeferencing solution, including platform position and attitude data, is computed by an Extended Kalman Filter (EKF), where first aircraft GPS data are processed in DGPS (Differential GPS) mode based on a nearby ground GPS base station (or network solution), and the DGPS results are feed back to the EKF to control the INS which provides the final georeferencing solution (Zhang *et al.*, 1994; Grejner-Brzezinska, 1999; Haala *et al.*, 2000; Tuo and Liu, 2005; Grejner-Brzezinska *et al.*, 2005). In addition, sensor alignment information, which is obtained by accurate boresight calibration, is applied to the platform georeferencing data to derive the exterior orientation parameters (EOPs) of the camera.

While GPS is generally available, there are certain rare circumstances that direct georeferencing is not available, such as in GPS denied environment. In fact, GPS signals could be vulnerable to interference, such as jamming, broadcast television, ultrawide-band communications, over-the-horizon radar and cellular telephones (Carroll, 2001). In addition, there are remote, inaccessible areas that lack a geodetic infrastructure and thus GPS/INS-based georeferencing is not always feasible. In these cases, EOPs have to be estimated through the indirect or image referenced georeferencing technique.

Previously acquired and processed geospatial data are a good source for ground control that can be used not only for airborne image georeferencing (Dowman, 1998; Lin and Medioni, 2007; Cariou and Chehdi, 2008; Oh *et al.*, 2010), but also for aircraft navigation (Oh *et al.*, 2006; Conte and Doherty, 2009). The requirements for such reference data include high positional accuracy, and geometric and radiometric properties similar to target airborne imagery. From the various geospatial images obtained from different sensors, high resolution satellite images have clear advantages due to their uniform global accessibility.

Since high resolutions satellite images meet the main requirements in terms of the spatial and spectral resolution and positioning accuracy, this study proposes their use for georeferencing of airborne pushbroom imagery. Note that the spatial resolution of satellite images is lower than that of airborne imagery, yet the currently allowed 50 cm satellite image resolution has a good potential for image matching.

Figure 1 depicts a GPS denied situation. At the epoch t_0, direct georeferencing becomes unavailable, as GPS is denied and there is no external information until t_1. Between t_1 and t_2, there is reference image data available and using common features, georeferencing is possible. Between the epochs t_2 and t_3, the image referenced georeferencing may not be feasible when there are not enough image features in the reference data, such as in forested areas (Oh *et al.*, 2010).
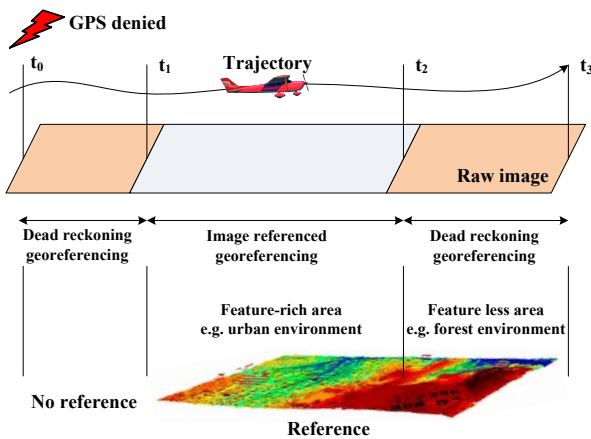
---

* Corresponding author.

In: Wagner W., Székely, B. (eds.): ISPRS TC VII Symposium – 100 Years ISPRS, Vienna, Austria, July 5–7, 2010, IAPRS, Vol. XXXVIII, Part 7B

Contents   Author Index   Keyword Index

Figure 1. Georeferencing in GPS denied situation

Satellite	Resolution [m]	Revisit time [day]	Swath width [km]
IKONOS (1999)	0.82	3~5	11.3
EROS-A (2000)	1.8	3~4	14
Quickbird (2001)	0.61	1~3.5	16.5
SPOT-5 (2002)	2.5	2~3	60
OrbView-3 (2003)	1	~3	8
FORMOSAT-2(2004)	2	1	24
CARTOSAT-1(2005)	2.5	5	30
ALOS PRISM (2006)	2.5	2~46	35
KOMPSAT-2 (2006)	1	4	15
EROS-B (2006)	0.70	3~4	7
WorldView-1 (2007)	0.50	4.6 (60cm)	17.6
CARTOSAT-2(2008)	0.80	4~5	9.6
GeoEye-1 (2008)	0.41	2.8 (50cm)	15.2
WorldView-2 (2009)	0.46	3.7 (52cm)	17.6

Table 1. Current high-resolution satellite imaging systems

In a recent research for automatic georeferencing of airborne pushbroom scanner by Cariou and Chehdi (2008), the reference data is transformed into the acquired image domain using the initial EOPs from INS, and then mutual information is computed between the transformed reference and acquired image. Through iteration of this computation and image transformation, a pixel-to-pixel correspondence is obtained and used for estimating yaw angle, and small bias in roll, pitch and height constant. This approach requires good initial EOPs from the INS and is computation intensive as a large number of iterative image transformations are needed.

This study proposes the combination of SURF (Speeded-Up Robust Features) (Bay *et al*., 2008) and RANSAC (Fischler and Bolles, 1981) for robust image matching, and the collinearity equation camera model with the Gauss-Markov stochastic error model for the trajectory modeling of the airborne pushbroom camera. The paper is structured as follows. First, the proposed method is presented, including a brief description on the image matching and platform trajectory modeling. Second, experimental results on simulation data are discussed, followed by a brief conclusion.

2. HIGH RESOLUTION SATELLITE IMAGE AS GROUND CONTROL INFORMATION

Since IKONOS-2 showed its potential in the commercial satellite image market, many high-resolution satellite imaging systems have been launched, see Table 1. The specification of high-resolution satellite images is listed in terms of its spatial, temporal resolution, and swath width. Note that many satellites provide sub-meter resolution with large swath width of more than 10 km. In addition, positioning accuracy has seen a steady increase over the years. For example, GeoEye-1 provides RPC with positional accuracy up to 2 m of circular error at a 90% confidence level (CE90) without GCP in the case of stereo images, and sub-meter accuracy could be achieved using a bias-compensation RFM model with a single GCP (Fraser and Ravanbakhsh, 2009). Moreover, higher performance satellites will be launched in the near future such as CARTOSAT-3, EROS-C, and GeoEye-2. These attractive capabilities motivate the idea of using high resolution satellite images as ground control information for other geospatial images, such as aerial images. In the navigation field, research has started on testing and suggesting the use of satellite imagery to support UAV navigation (Sim *et al*., 2002; Conte and Doherty, 2008).

3. PROPOSED METHOD

Figure 2 shows the flowchart of the proposed method. As direct georeferencing is unavailable, due to GPS denied condition, and the reference data becomes available, short duration of HSI and INS is processed for georeferencing purposes. Though the INS data is drifting without georeferencing fixes, it can still provide good approximation for georeferencing, and thus reference data is windowed with an error margin, so the image matching with the raw HSI is limited to a smaller reference area (subset). During image matching, SURF is utilized with RANSAC to mitigate the effect of mismatched points. Successful image matching provides ground control information for each extracted raw image point, and thus the trajectory and attitude are estimated based on this information.
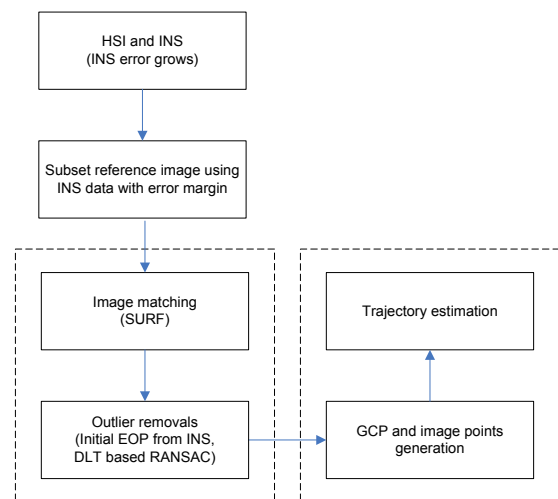

Figure 2. Flowchart of the proposed approach

3.1 Subset ROI reference data

Since images used as reference data tend to be large, it would take too much time and require a lot computer power if the whole reference image is used for image matching. fortunately, the INS-based estimation of location can provide good approximation to obtain a region of interest (ROI), using the inverse form of collinearity equation. The ground coordinate of ROI can be determined from Equation 1. The ground height information could be selected as a constant value from knowledge about the target area; note that error of the height will be compensated in the error margin terms.

In: Wagner W., Székely, B. (eds.): ISPRS TC VII Symposium – 100 Years ISPRS, Vienna, Austria, July 5–7, 2010, IAPRS, Vol. XXXVIII, Part 7B

Contents   Author Index   Keyword Index

$$X = (Z - Z_L)\frac{U}{W} + X_L + b_X \qquad (1)$$

$$Y = (Z - Z_L)\frac{V}{W} + Y_L + b_Y$$

$$\begin{bmatrix} U \\ V \\ W \end{bmatrix} = M^T \begin{bmatrix} x \\ y \\ -f \end{bmatrix}$$

where,

x, y : image coordinate of an object point
$[X \ Y \ Z]^T$: ground coordinates of an object point
$[X_L \ Y_L \ Z_L]^T$: the camera perspective center's coordinates
M : the rotation matrix from ground to camera coordinates frame consisting of roll, pitch, and yaw
f : camera focal length
b_X, b_Y : error margin which incorporate errors of INS and Z

3.2 Image matching (SURF with RANSAC)

Robust and accurate image matching is difficult due to significant differences between aerial and reference images. Therefore, robust SURF (Bay *et al.*, 2008) is utilized with RANSAC (Fischler and Bolles, 1981) to mitigate the effect of mismatching points.

SURF is a fast, scale and rotation invariant interest point detector and descriptor motivated by SIFT (Scale-Invariant Feature Transform; Lowe, 1999) which is one of the most popular point feature extraction and matching methods since it has been recognized to be very reliable and invariant to changes in imaging conditions. To increase the processing speed, SURF utilizes integral image, Laplacian-based indexing, and wavelets, and SURF is known to execute several times faster than SIFT.

RANSAC is a technique to estimate parameters of a model through iteration from a set of observations containing outliers. Model parameters are estimated from a randomly selected observation set and then every observation is tested if it fits to the model, and is added to the consensus set if it does. In an iterative process, a new consensus set is obtained and a better model is estimated. RANSAC is useful especially when the number of outliers is large. In contrast, other robust techniques, such as the least squares' residual check or Baarda's data snooping (Baarda, 1968) have practical limitations. Note that it is important to select the geometric model to constrain the mismatching in RANSAC. In this study, DLT (Direct Linear Transform) is used because data for small time span is assumed.

3.3 Platform modelling

When point features are used, platform modeling is generally performed using the collinearity equation, see Equation 2. The collinearity equation can be linearized to form a linear observation equation. The EOP parameters can be estimated iteratively using the above linearized observation equation through least square adjustment.

$$F_x = x + f\frac{U}{W} = 0 \qquad (2)$$

$$F_y = y + f\frac{V}{W} = 0$$

In the Gauss-Markov (GM) model proposed here, each image line has six unique EOP parameters. However, the EOP parameters in adjacent lines are stochastically constrained, thus the first order Gauss-Markov model can be expressed by Equations 3 and 4.

$$x_k = A_1 x_{k-1} + w \qquad (3)$$

where,

$$A_1 = \text{cov}(x_k, x_{k-1})\text{cov}(x_k, x_{k-1})^{-1} = e^{-\beta_1 \Delta t} \qquad (4)$$

w : white noise

Note that the correlation time is $1/\beta_1$. Denoting $\beta_1 \Delta t$ as S, the stochastic constraint equation can be derived.

$$F_{G1} = e^{-s_{X_L}} \Delta X_{L(i-1)} - \Delta X_{L(i)} = 0$$

$$F_{G2} = e^{-s_{Y_L}} \Delta Y_{L(i-1)} - \Delta Y_{L(i)} = 0$$

$$F_{G3} = e^{-s_{Z_L}} \Delta Z_{L(i-1)} - \Delta Z_{L(i)} = 0 \qquad (5)$$

$$F_{G4} = e^{-s_\omega} \Delta \omega_{(i-1)} - \Delta \omega_{(i)} = 0$$

$$F_{G5} = e^{-s_\phi} \Delta \phi_{(i-1)} - \Delta \phi_{(i)} = 0$$

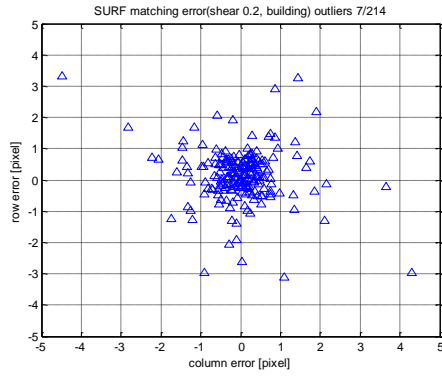$$F_{G6} = e^{-s_\kappa} \Delta \kappa_{(i-1)} - \Delta \kappa_{(i)} = 0$$

where,
i : line number in the image
s : coefficient for each EOP

Solving the platform modeling with the above stochastic constraint yields a total of $6L$ EOP parameters where L is the total number of lines in the image. Lee (1999) mentioned that the number of unknown EOP parameters could be reduced from $6L$ to 6 through equation reduction. Therefore, three control points could generate a unique solution.
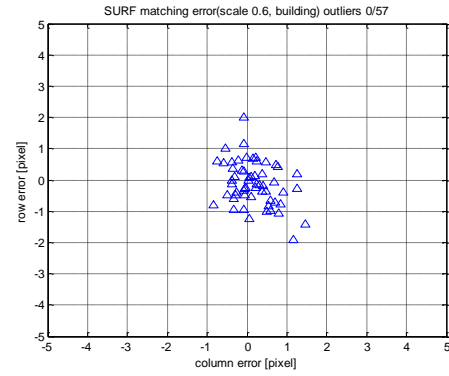
4. SIMULATION TEST

4.1 SURF image matching and outlier removal test

SURF matching with RANSAC outlier removal was tested on simulated images from CASI-1500 hyperspectral imagery (ITRES). The test images were generated by applying image various transformations, such as shear, rotation, intensity and resolution differences to simulate different imaging conditions between the target reference images. After image simulation, SURF matching between original and simulated images was performed and the accuracy was analyzed; the results for shear and resolution differences are presented in Figure 3.
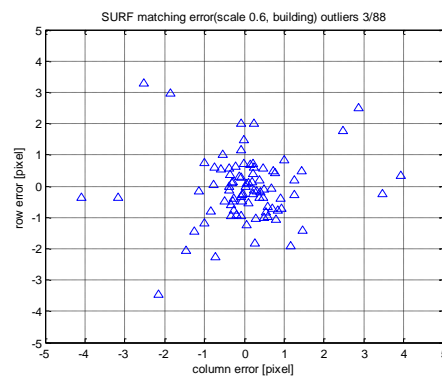
In: Wagner W., Székely, B. (eds.): ISPRS TC VII Symposium – 100 Years ISPRS, Vienna, Austria, July 5–7, 2010, IAPRS, Vol. XXXVIII, Part 7B

Contents   Author Index   Keyword Index

(a)

(b)

Figure 3. SURF image matching results for (a): 0.2 image shear, and (b): 0.6 times image scale difference

While most matching points are reasonably accurate, several low accuracy points are observed; the number of outliers with accuracy of lower than 5 pixels is shown in the title. Obviously, they should be filtered out to be used as ground control information. Therefore, RANSAC was tested for the same data set and the accuracy is shown in Figure 4. Note that low accuracy points and outliers are successfully removed. Most points show matching accuracy less than one-pixel. These test results show the potential of the method for matching between HSI and satellite images.

(a)

(b)

Figure 4. RANSAC tests for (a): 0.2 image shear, and (b): 0.6 times image scale difference

4.2 EOP Simulation

The platform modeling test was performed using simulated data. The camera specification used for simulation is presented in Table 2.

| Camera type	Pushbroom
Focal length	79 mm
Pixel size	40 micron
Image size	Row: 1280, Col: 320
Imaging rate	80 lines/sec

Table 2. Camera specification

Given reference EOPs, the INS-only EOPs were simulated assuming drift errors. During 16 sec (1280 lines), the position error was simulated to increase to 8 m and the attitude drifted reached 0.25°. The simulated EOPs are shown in Figure 6.

4.3 Platform modeling test

The ground control points are normally generated by image matching based on SURF with RANSAC between the aerial pushbroom and satellite images. For this study, a total of 186 ground control points were simulated in an irregular distribution, as shown in Figure 5.

The INS-only EOPs are used as initial EOP values for the platform trajectory modeling. The EOPs estimated using the GM model are presented in Figure 6. Perspective center positions follow the initial EOPs values but the attitude accuracy slightly improved. The yaw angle could be estimated well.
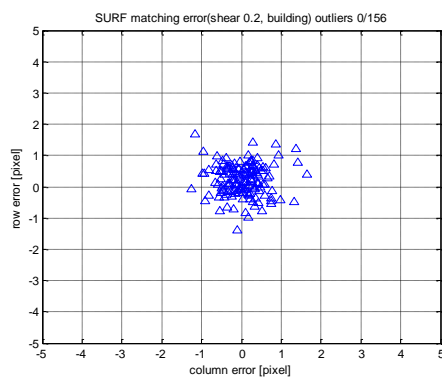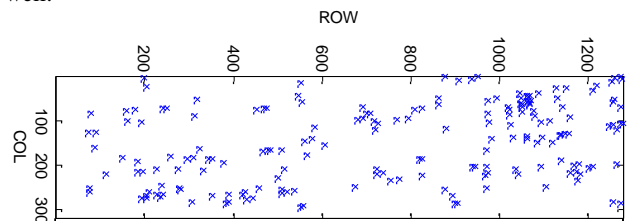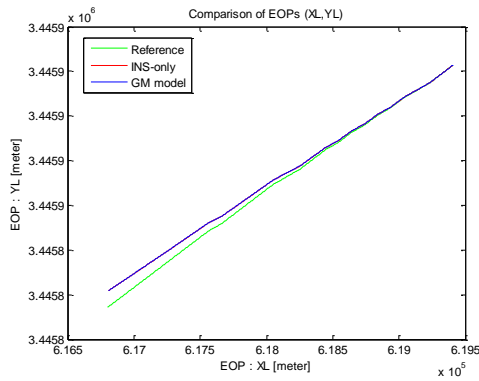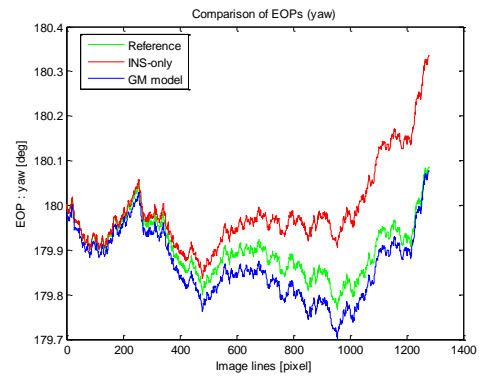

Figure 5. Distribution of simulated ground control points (assumed generated by the image matching)

In: Wagner W., Székely, B. (eds.): ISPRS TC VII Symposium – 100 Years ISPRS, Vienna, Austria, July 5–7, 2010, IAPRS, Vol. XXXVIII, Part 7B

Contents   Author Index   Keyword Index

(a)

(b)

(c)
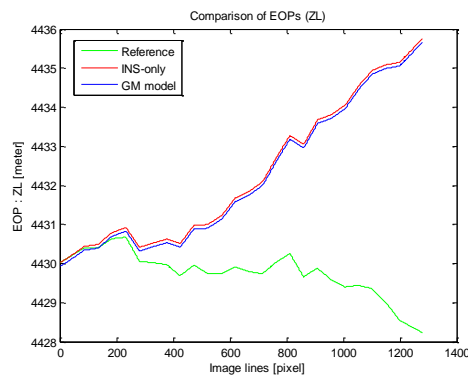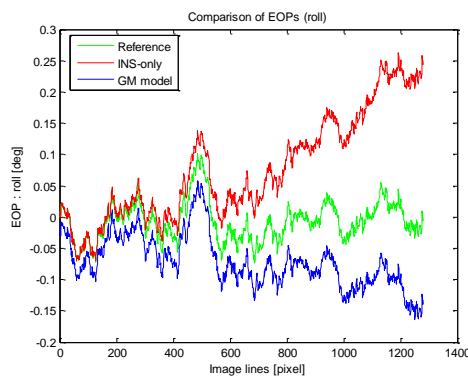

(d)

(e)
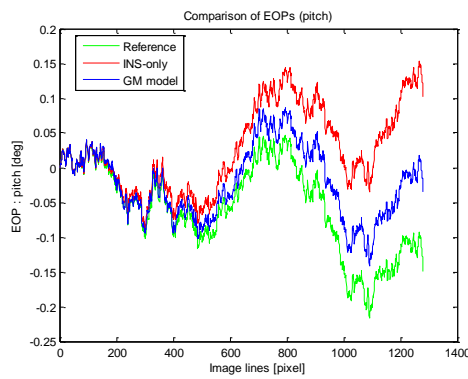
Figure 6. Platform modeling results, (a): X and Y, (b): Z, (c): roll, (d): pitch, and (e) yaw

4.4 Georeferencing accuracy

Since the image is monoscopic, the 3D ground restitution accuracy cannot be analyzed. Therefore, horizontal ground accuracy is analyzed by projecting image points to the ground with given ground height information. Each image point is projected to the ground using the estimated EOPs and the horizontal accuracy was computed. Table 3 shows the RMSE of the computed horizontal accuracy. The georeferencing result was accurate as the RMSE of ground coordinates is less than 1 m, while Gauss-Markov modeling did not accurately estimate the perspective center positions and attitudes due to correlation between EOP parameters.

RMSE	X [m]	Y [m]	# of points
	0.47	0.16	186

Table 3. Ground accuracy of the modeling

5. CONCLUSION

Airborne HSI systems have shown excellent performance in many commercial and defence applications. Most of the state-of-the-art systems are of the pushbroom camera type, and the georeferencing of these systems heavily relies on the GPS/INS based direct georeferencing. Under some rare circumstances, direct georeferencing may not be feasible, such as GPS denied situations. This study addresses these situations and proposes an image referenced georeferencing solution for pushbroom sensors. The approach is based on using high resolution satellite imagery, and the effort was motivated by the attractive properties of high-resolution satellite images, including high geolocation performance and image acquisition capability. The proposed method utilizes robust image matching, using a combination of the SURF and RANSAC techniques, and the platform modeling is based on the Gauss-Markov stochastic model.

The SURF image matching performance with RANSAC was tested using simulated images and showed robustness by successfully mitigating low accuracy matching points. Next, the pushbroom sensor platform modeling was tested using simulated EOPs data and ground controls, which were obtained by simulated image matching. Test results indicated a good performance potential of the approach by showing high ground accuracy while EOPs could be estimated moderately.

In: Wagner W., Székely, B. (eds.): ISPRS TC VII Symposium – 100 Years ISPRS, Vienna, Austria, July 5–7, 2010, IAPRS, Vol. XXXVIII, Part 7B

| Contents | Author Index | Keyword Index |

6. REFERENCE

References from Journals:

Bay, H., A. Ess, T. Tuytelaars, L.V. Gool, 2008. SURF: Speeded Up Robust Features, *Computer Vision and Image Understanding (CVIU)*, 110(3): 346-359.

Cariou, Claude., and K. Chehdi, 2008, Automatic Georeferencing of Airborne Pushbroom Scanner Images With Missing Ancillary Data Using Mutual Information, *IEEE Transactions on Geoscience and Remote Sensing*, 46(5), pp.1290-1300.

Conte, Gianpaolo., and P. Doherty, 2009, Vision-Based Unmanned Aerial Vehicle Navigation Using Geo-Referenced Information, *Journal on Advances in Signal Processing*, Vol. 2009.

Dowman, I.J., 1998, Automating Image Registration and Absolute Orientation: Solutions and Problems, *Photogrammetric Record*, 16(91), pp.5–18.

Fischler, M. A. and R. C. Bolles, 1981. Random Sample Consensus: A Paradigm for Model Fitting with Applications to Image Analysis and Automated Cartography, *Communications of the ACM*. 24: 381–395.

Fraser, C.S., and H.B. Hanley, 2005. Bias-compensated RPCs for sensor orientation of high-resolution satellite imagery. *Photogrammetric Engineering & Remote Sensing*, 71(8):909-915.

Grejner-Brzezinska, D. A., 1999. Direct exterior orientation of airborne imagery with GPS/INS system: Performance analysis, *Navigation*, 46(4):261-270.

Grejner-Brzezinska, D. A., C. Toth, Y.D. Yi, 2005, On improving navigation accuracy of GPS/INS systems, *Photogrammetric Engineering & Remote Sensing*, 71(4), pp.377-389.

Oh, Y.S., D.G. Sim, R.H. Park, R.C. Kim, S.U. Lee, and I.C. Kim, 2006, Absolute position estimation using IRS satellite images, *ISPRS Journal of Photogrammetry & Remote Sensing*, 60 (2006), pp.256–268.

Sim, D.G., R.H. Park, R.C. Kim, S.U. Lee, and I.C. Kim, 2002, Integrated Position Estimation Using Aerial Image Sequences, *IEEE Transactions on Pattern Analysis and Machine Intelligence*, 24(1), pp.1-18.

Tuo, Hongya., Y. Liu, 2005, A new coarse-to-fine rectification algorithm for airborne push-broom hyperspectral images, *Pattern Recognition Letters*, 26(11), pp.1782-1791.

References from Books:

Baarda, W. 1968. *A testing procedure for use in geodetic networks*, Netherlands Geodetic Commission, Publications on Geodesy, New Series, Vol. 2, No. 5, Delft, 1968.

References from Other Literature:

Carroll, J., 2001. Vulnerability assessment of the transportation infrastructure relying on the global positioning system, Technical report, Volpe National Transportation Systems Center, August 2001. Report for US Department of Transportation.

Haala, Norbert., D. Fritsch, D. Stallmann, and M. Cramer, 2000, On the Performance of Digital Airborne Pushbroom Cameras for Photogrammetric Data Processing – A Case Study, *IAPRS*, Vol. XXXIII, Amsterdam.

Lee, C. N., 1999. Mathematical modeling of airborne pushbroom imagery using point and linear features, Doctoral dissertation, PhD diss, Purdue University.

Lin, Yuping., and G. Medioni, 2007, Map-Enhanced UAV Image Sequence Registration and Synchronization of Multiple Image Sequences, *IEEE Conference on Computer Vision and Pattern Recognition*, 17-22 June 2007. pp.1-7.

Lowe, D.G., 1999. Object recognition from local scale-invariant features. In: *Proceedings International Conferences on Computer Vision*, Corfu, Greece, pp.1150-1157.

Oh, Jaehong., C. K. Toth and D. A. Grejner-Brzezinska, 2010, Automatic Geo-referencing of Aerial images using High-resolution Stereo Satellite Images, *ASPRS 2010 Annual Conference*, San Diego, CA, April 26-30.

Skaloud, Jan., 1999, Problems in Direct-Georeferencing by INS/DGPS in the Airborne Environment, *ISPRS Workshop on 'Direct versus Indirect Methods of Sensor Orientation'* WG III/1, Barcelona 25-26.

Zhang, W., J. Albertz, and Z. Li, 1994. Rectification of Airborne Line-Scanner Imagery Utilizing Flight Parameters. *In Proceedings of the First International Airborne Remote Sensing Conference and Exhibition*, Strasbourg, Vol.2, pp. 447–456, ERIM, Ann Arbor.